A&A 391, 275–285 (2002)
DOI: 10.1051/0004-6361:20020786

Astronomy & Astrophysics

$C^{18}O$ abundance in the nearby globule Barnard 68⋆

S. Hotzel[1,2], J. Harju[2], M. Juvela[2], K. Mattila[2], and L. K. Haikala[3]

[1] Max-Planck-Institut für Astronomie, Königstuhl 17, 69117 Heidelberg, Germany
[2] Observatory, PO Box 14, 00014 University of Helsinki, Finland
[3] Swedish-ESO Submillimetre Telescope, European Southern Observatory, Casilla 19001, Santiago, Chile

Received 23 January 2002 / Accepted 23 May 2002

Abstract. We have studied the radial variation of the CO abundance in the nearby isolated globule Barnard 68 (B68). For this purpose, B68 was mapped in the three rotational lines $^{13}CO(J = 1–0)$, $C^{18}O(J = 1–0)$ and $C^{18}O(J = 2–1)$. Using the recent discovery of Alves et al. (2001) that the density structure of B68 agrees with the prediction for a pressure bound distribution of isothermal gas in hydrostatic equilibrium (Bonnor-Ebert sphere), we show that the flat CO column density distribution can be explained by molecular depletion. By combining the physical model with the observed CO column density profile, it was found that the density dependence of the CO depletion factor f_d can be well fitted with the law $f_d = 1 + \text{const.}\, n(H_2)$, which is consistent with an equilibrium between the accretion and the desorption processes. In the cloud centre, between 0.5% and 5% of all CO molecules are in the gas phase. Our observations suggest a kinetic temperature of ≈8 K. In combination with the assumption that B68 is a Bonnor-Ebert sphere, this leads to a distance of 80 pc. The cloud mass consistent with these values is 0.7 $M_\odot$, considerably less than previously estimated. We find in B68 no clear deviance of the near-infrared reddening efficiency of dust grains per unit H_2 column density with respect to values derived in diffuse clouds.

Key words. ISM: individual objects: Barnard 68 – ISM: abundances – ISM: molecules – ISM: dust, extinction

1. Introduction

It was recently discovered by Alves et al. (2001) that the circularly-averaged visual extinction profile of the globule Barnard 68 (B68)[1] agrees remarkably well with the predictions for an isothermal sphere in hydrostatic equilibrium or a so-called Bonnor-Ebert sphere (BES). The suggested structural simplicity makes B68 particularly favourable for the determination of physical parameters and chemical abundances, and, since the cloud probably represents a state prior to protostellar collapse, for studying processes influencing star formation.

One important process is gas-phase depletion of molecules through freezing out onto dust grains. CO depletion changes the chemical and physical structure of globules by affecting the deuterium fractionation and the ionization degree (Caselli et al. 1998), the cooling efficiency and thermal balance, and the gas phase chemical composition. Additionally, depletion must be taken into account when using CO spectroscopy to trace molecular hydrogen. Observational evidence for molecular accretion onto dust grains comes from the detection of absorption features of molecular ices (e.g. Tielens et al. 1991), the observation of chemical fractionation between more and less volatile molecular species (e.g. Zhou et al. 1989) and the comparison of column densities of gaseous CO and dust (e.g. Caselli et al. 1999).

B68 was observed earlier in CO (Avery et al. 1987) and NH_3 (Bourke et al. 1995; Lemme et al. 1996), which yielded temperature and density estimates of the globule. Avery et al. (1987) used multi-level CO and $^{13}CO(J = 1–0)$ observations to deduce an outward increasing kinetic temperature between 6 and 11 K. Bourke et al. (1995) observed B68 in the $(J, K) = (1, 1)$ and $(2, 2)$ inversion lines of ammonia and derived a kinetic temperature of 16 K and an H_2 number density of 9.1×10^3 cm^{-3}.

The distance D to B68 cited by most authors originates from Bok & McCarthy (1974), who allocated $D = 200$ pc because of the globule's proximity to the Ophiuchus complex. However, the distance to the Ophiuchus dark clouds was redetermined by de Geus et al. (1989), who found the complex extending from $D = 80$ to 170 pc with a central value of 125 pc. Other determinations of the distance to the centre of the complex also fall in the $D = 125$–200 pc range (Chini 1981; Straizys 1984). It should be emphasised that no distance estimate for B68 itself is available, and due to the lack of foreground stars would be difficult to obtain using classical methods.

Alves et al. (2001) used H and K imaging of B68 to determine the near-infrared (NIR) colours of thousands of background stars. These extinction measurements provided a high

Send offprint requests to: S. Hotzel,
e-mail: hotzel@astro.helsinki.fi

⋆ Based on observations made with the Swedish-ESO Submillimetre Telescope (SEST), Chile.

[1] Discovered by Barnard (1919), other identifiers for B68 are LDN 57 (Lynds 1962) and [CB88] 82 (Clemens & Barvainis 1988). A wrong identification of [CB88] 82 with LDN 55 can be found in the literature, which is probably due to unprecise coordinates in the catalogue of Lynds (1962).

resolution column density profile and yielded a physical cloud model for B68. These achievements allow us to study CO depletion in more detail than done before in other objects, where both CO and H_2 density distributions are described by ad hoc models.

In the present study we determine the CO column density distribution and the degree of CO depletion in B68 by using isotopic CO line observations. Combining our observations with the extinction measurements of Alves et al. (2001), we are able to quantify the CO abundance as a function of density and compare the observed depletion with theoretical expectations. We also give an estimate for the cloud's kinetic temperature. Using this and the assumption of a BES we propose new values for the cloud's distance, mass and H_2-to-extinction ratio.

2. B68 as Bonnor-Ebert cloud

Throughout this paper, we make extensive use of the dust column density profile measured by Alves et al. (2001) and in parts also take up their proposal of B68 being a Bonnor-Ebert sphere (BES). In order to make transparent which assumptions are involved in deriving various quantities, we summarise in this section the concept of Bonnor-Ebert spheres and discuss its applicability to B68.

Assuming an isothermal, spherically symmetric distribution of gas in hydrostatic equilibrium, a cloud's density profile is governed by Eqs. (374) and (375) of Chandrasekhar (1939, p.156). As Bonnor (1956) and Ebert (1955) pointed out, these equations have a family of solutions characterised by the nondimensional radial parameter $\xi_{\rm max}$, if the sphere is bound by a fixed external pressure $P_{\rm R}$. They also discovered that such a gaseous configuration is unstable to gravitational collapse if $\xi_{\rm max} > 6.5$. With R being the radius where the pressure $P(r)$ has dropped to $P_{\rm R}$, the physical parameters are determined by the scaling relation $\xi_{\rm max} = \xi(r = R) = \sqrt{4\pi G \rho_{\rm c}} R/a$, where $\rho_{\rm c}$ is the central density, a the isothermal sound speed and G the gravitational constant.

In practice, the radius of a cloud cannot be directly observed, but only its angular diameter $\theta_{\rm R}$ and in certain circumstances its distance D. Using the mean molecular weight m and the central number density $n_{\rm c}$ to write $\rho_{\rm c} = m n_{\rm c}$ and $a = \sqrt{kT/m}$, where k is the Boltzmann constant and $T \equiv T_{\rm kin}$ the kinetic temperature, we can express the relation between the physical parameters of a BES as

$$\frac{\xi_{\rm max}}{\theta_{\rm R}} = D \sqrt{\frac{4\pi G n_{\rm c}}{kT}}\, m\,. \tag{1}$$

The column density profile of a BES is determined by numerical integration. The column density towards the centre is $N_{\rm c} = K\, n_{\rm c}\, D\, \theta_{\rm R}$, where the constant K depends only on $\xi_{\rm max}$. The shape of the density profile as well as the shape of the column density profile depend only on $\xi_{\rm max}$, i.e. the normalised profiles $n/n_{\rm c}$ vs. $\theta/\theta_{\rm R}$ and $N/N_{\rm c}$ vs. $\theta/\theta_{\rm R}$ are fully determined by $\xi_{\rm max}$. Vice versa, if the normalised column density profile of a cloud is measured, $\xi_{\rm max}$ can be determined without any knowledge of any of the parameters on the right hand side of Eq. (1). Not even $\theta_{\rm R}$ has to be known for this, but naturally $\theta_{\rm R}$ comes with the astrometric calibration of the CCD image.

Alves et al. (2001) determined the extinction profile of B68 and found it to have the same shape as the column density profile of a BES with $\xi_{\rm max} = 6.9$. Does this mean that B68 actually *is* a BES? First of all, one has to assume that the shape of the *gas* column density profile has been measured, i.e. $N_{\rm gas} \propto E(H-K)$. Except for Sect. 4.1.2, all results of this paper implicitly fall back on this assumption. But despite having the column (and hence number) density profile of a BES, the globule may still not be a BES in the sense that it may not be isothermal, it may not be in hydrostatic equilibrium and it may not be in equilibrium altogether. It is safe to say that B68 cannot be a perfect BES for a number of reasons: 1) Its shape is not perfectly circulary symmetric. 2) The molecular line-widths show that a small microturbulent velocity field is present. 3) The measured $\xi_{\rm max}$ is larger than the critical value, i.e. B68 is unstable to gravitational collapse unless some additional support mechanism, e.g. a magnetic field, plays a role. Nevertheless, in the framework of inevitable idealisations in astronomy, the BES model fits B68 certainly to some degree (as the density profile fits near-perfectly). We will resume the BES model and discuss the conclusion from applying it to B68 in Sect. 6.2. Therefore we calculate the numerical constants involved in the following paragraphs. Note that up to and including Sect. 6.1 we refer with "cloud model" and "BES profile" to the fitted (column) density profile, which is based on the raw observations of Alves et al. (2001) and does not require the hydrostatic equilibrium assumption.

The extinction profile of B68 only deviates noticeably from a BES profile in the outermost parts (for $r > 100''$, see Fig. 2 of Alves et al. 2001). As the fitting parameters, particularly $\theta_{\rm R}$, change considerably if one tries to scale the BES profile to also those data points, we have done a χ^2-fit to the data of Alves et al. (2001, who kindly provided us with the data), deliberately ignoring data points at $r > 100''$ at this stage. The lowest χ^2 was found for $\xi_{\rm max} = 6.99$, which corresponds to a centre-to-edge density contrast of 17.1. The scaling parameters for this particular BES extinction profile are $\theta_{\rm R} = 106.35''$ and $A_{\rm V} = 30.3$ mag (see also Fig. 4a). The actual peak extinction value is not needed in Eq. (1), but will be used in Sects. 5 and 6 to derive the H_2-to-extinction ratio in B68. Varying $\xi_{\rm max}$ by one decimal increases χ^2 by 2%, while the scaling parameters $\theta_{\rm R}$ and $A_{\rm V}$ are modified by 0.6% and 0.3% respectively. The density contrast, being an increasing function of $\xi_{\rm max}$, is the least precise parameter, changing between 16.5 and 17.7 for the given variation of $\xi_{\rm max}$.

For a BES with $\xi_{\rm max} = 6.99$ and $\theta_{\rm R} = 106.35''$, we have calculated the following values for the radius R, the central gas particle number density $n_{\rm c}$, the peak column density $N_{\rm c}$, the total mass M and the external pressure $P_{\rm R}$:

$$\begin{array}{lll} R = 10635\ {\rm AU} & \mathcal{D} & \\ n_{\rm c} = 2.090 \times 10^5\ {\rm cm^{-3}} & \mathcal{D}^{-2} & \mathcal{T} \\ N_{\rm c} = 2.590 \times 10^{22}\ {\rm cm^{-2}} & \mathcal{D}^{-1} & \mathcal{T} \\ M = 1.049\ M_\odot & \mathcal{D} & \mathcal{T} \\ P_{\rm R} = 1.687 \times 10^{12}\ {\rm Pa} & \mathcal{D}^{-2} & \mathcal{T}^{-2}, \end{array} \tag{2}$$

abbreviating $\mathcal{D} = \frac{D}{100\,\mathrm{pc}}$ and $\mathcal{T} = \frac{T}{10\,\mathrm{K}}$. The external pressure follows from n_c, as the centre-to-edge density contrast only depends on ξ_{max}.

We assume H_2 and He are the only species contributing substantially to mass and pressure, with a fractional helium abundance of $n_{He}/n_{H_2} = 0.2$. Under this assumption, the mean molecular weight is $m = 2.329\,m_H$ (m_H being the atomic hydrogen mass). Throughout this paper, we use the commonly used rounded value $m = 2.33\,m_H$. For other values of m, the quantities in Eq. (2) have to be scaled as $n_c \propto m^{-2}$, $N_c \propto m^{-2}$, $M \propto m^{-1}$ and $P_R \propto m^{-2}$.

If two of the three remaining unknown variables (D, T and n_c) in Eq. (1) are known, the third one follows from Eq. (1) and the cloud model is fixed. This way we first calculated n_c in Eq. (2), then from the fixed cloud model we determined N_c and M. If all three variables D, T and n_c can be determined from observations, Eq. (1) allows a consistency check of the involved parameters. In practice, for a small globule like B68 both T and n_c can be determined to some accuracy e.g. by ammonia observations, while a distance estimate remains difficult due to the lack of foreground stars. In fact, Eq. (1) can be used to determine the distance under these circumstances.

3. Observations

The observations were carried out at the Swedish-ESO Submillimetre Telescope (SEST) in two runs: February 1993 and May 2000. During the first session we mapped B68 in the $^{13}CO(J = 1–0)$ and $C^{18}O(J = 1–0)$ lines at 110.2 and 109.8 GHz, respectively. The map grid spacing was 20″ in the cloud centre and 40″ in the outer parts. The receiver used during these earlier observations was a 3 mm Schottky mixer dual channel receiver. By using two mixers tuned to the same frequency we observed orthogonal polarizations simultaneously. The system temperature, T_{SYS}, reduced to outside of the atmosphere, ranged from 300 to 400 K. In the mapping the observing time per position was typically 2 min, which resulted in an rms noise level of about 0.1 K. During the second period in May 2000 we mapped the cloud in $C^{18}O(J = 1–0)$ and $C^{18}O(J = 2–1)$ at 109.8 and 219.6 GHz simultaneously with 3 and 1.3 mm SIS receivers. The grid spacing was 20″. The system temperatures at the two frequencies were around 160 and 260 K, and the observing time per position was typically 1 min. The rms noise level attained was typically 0.06 K at 3 mm and 0.1 K at 1.3 mm.

The half-power beam width (HPBW) of the antenna is 47″ at 110 GHz and 25″ at 220 GHz. The pointing and focus were checked at 3–4 hour intervals towards circumstellar $SiO(v = 1, J = 2–1)$ maser line sources, and the pointing accuracy was typically found to be 3″. The map was centred on RA $17^h19^m34\overset{s}{.}6$, Dec −23°46′34″ (1950.0). All observations were performed in the frequency switching mode. The two mixers used at the same time were connected to a 2000 channel acousto-optical spectrometer which was split in two bands of 43 MHz each. The AOS channel width corresponds to 0.12 km s^{-1} at 2.7 mm and 0.06 km s^{-1} at 1.37 mm. Further details of the SEST are available at `http://www.ls.eso.org/lasilla/Telescopes/SEST`.

Calibration was done by the chopper wheel method. To convert the observed antenna temperatures, T_A^*, to the radiation temperatures, T_R, the former were divided by the assumed source–beam coupling efficiences, $\eta_C = \int_{source} P_n d\Omega/\Omega_A$, where Ω_A is the beam solid angle of the antenna and P_n the normalised beam pattern. For η_C we adopted the main beam efficiences of the telescope interpolated to the frequencies used, i.e. 0.71 and 0.61 at 110 and 220 GHz, respectively. Our numerical estimates for η_C were in fact close to these values when the source was assumed to be disk-like with a radius of 100″.

Line area maps of the $C^{18}O$ transitions are presented in Fig. 1. Characteristic for the $C^{18}O(J = 1–0)$ line intensity distribution is a steep rise at the edge and a plateau at the centre of the globule. The $C^{18}O(J = 2–1)$ line area looks patchy with maxima at the eastern edge of the globule and the prominent "nose" (cmp. Fig. 3) in the southeast.

4. Estimation of the CO column densities

Two different approaches were used to estimate the CO column density distribution across the cloud. Firstly, we used the traditional way to derive column densities directly from the observed lines by assuming that the excitation temperature for each transition is constant along the line of sight (Sect. 4.1). Secondly, starting from the physical cloud model (see Sect. 2) we used the Monte Carlo radiative transfer program developed by Juvela (1997) to simulate the observed profiles from the cloud. The physical quantities were derived by fitting the calculated spectra to the observed ones (Sect. 4.2). In the following, the two methods and the results are described in detail.

4.1. Line of sight homogeneity

4.1.1. Assumptions

The assumption of a constant excitation temperature T_{ex} implies that either the cloud is homogenous (the density and the kinetic temperature are constant) or that the cloud is isothermal and the transition in question is thermalised. Even if this simplistic assumption is valid, the derivation of the excitation temperatures of the observed isotopic CO lines involves the following difficulties: 1) The $^{13}CO/C^{18}O$ abundance ratio X has been observed to change from cloud to cloud, and may also vary from the cloud surface to its interior parts. This depends on ^{13}C fractionation and selective photodissociation (see e.g. Bally & Langer 1982; Smith & Adams 1984). 2) The populations of the rotational levels of $C^{18}O$ may deviate from LTE, i.e. from the situation where a single value of T_{ex} describes the relative populations of all J-levels. The populations are controlled by the collisional excitation and selective photodissociation mechanisms, which depend on the rotational quantum number (Warin et al. 1996). According to Warin et al. (1996) the latter process causes that low-lying rotational levels are thermalised or overpopulated and higher levels are subthermally excited. In their model calculation for a dense dark cloud with a kinetic temperature of $T_{kin} = 10$ K (see their Figs. 6a–c), the excitation temperatures of both $C^{18}O(J = 1–0)$ and $^{13}CO(J = 1–0)$

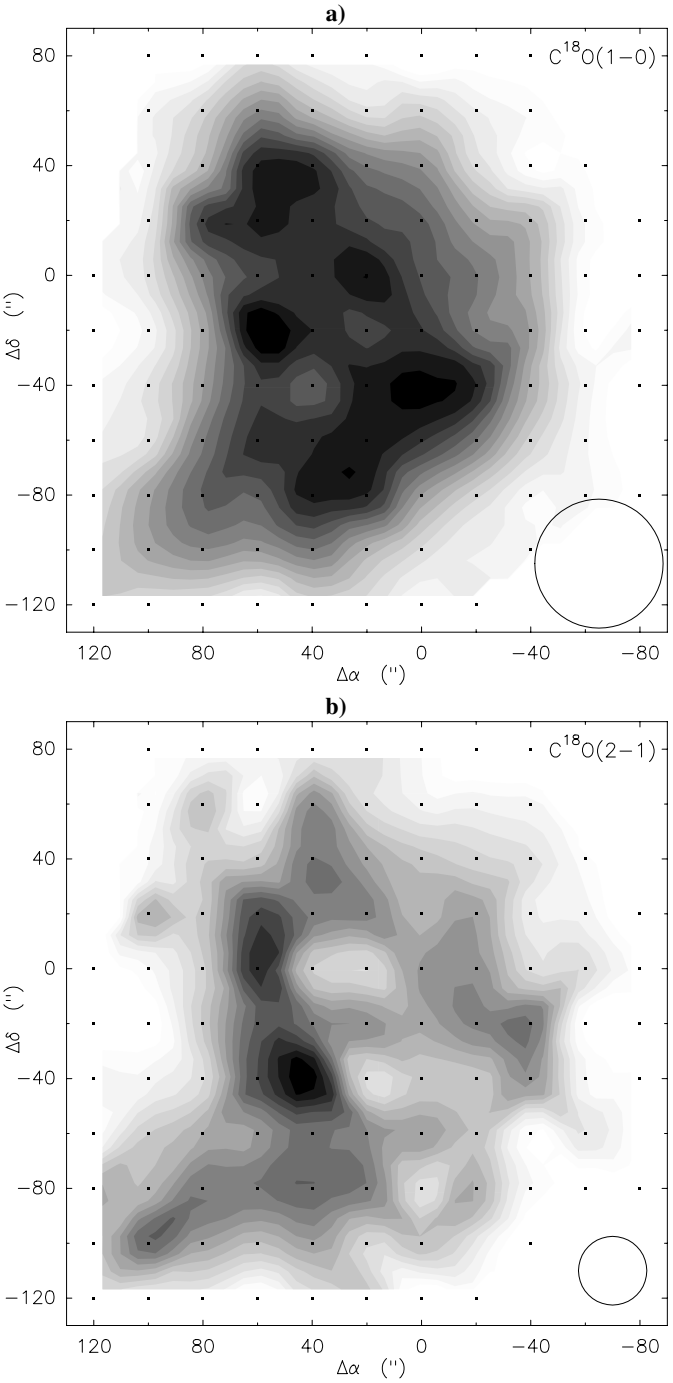

Fig. 1. $C^{18}O$ line area maps, centred on RA $17^h19^m34\overset{s}{.}6$, Dec $-23°46'34''$ (1950.0). The velocity range is 3.0–3.8 km s^{-1} and the beam (HPBW) is indicated in the lower right corner of each map. Small dots mark the positions actually observed. **a)** $C^{18}O(J = 1–0)$ line area. Grey scales range from 0.075 to 0.450 K km s^{-1} in steps of 0.025 K km s^{-1}. **b)** $C^{18}O(J = 2–1)$ line area. Grey scales range from 0.050 to 0.425 K km s^{-1} in steps of 0.025 K km s^{-1}.

lie close to T_{kin}, whereas $T_{ex}(J = 2–1)$ and all higher transitions of $C^{18}O$ settle between 6 and 7 K.

In the derivation of the $C^{18}O$ column densities we have made the following assumptions:

1. the $C^{18}O(J = 1–0)$ and $^{13}CO(J = 1–0)$ transitions have the same excitation temperature $T_{ex}(J = 1–0)$,

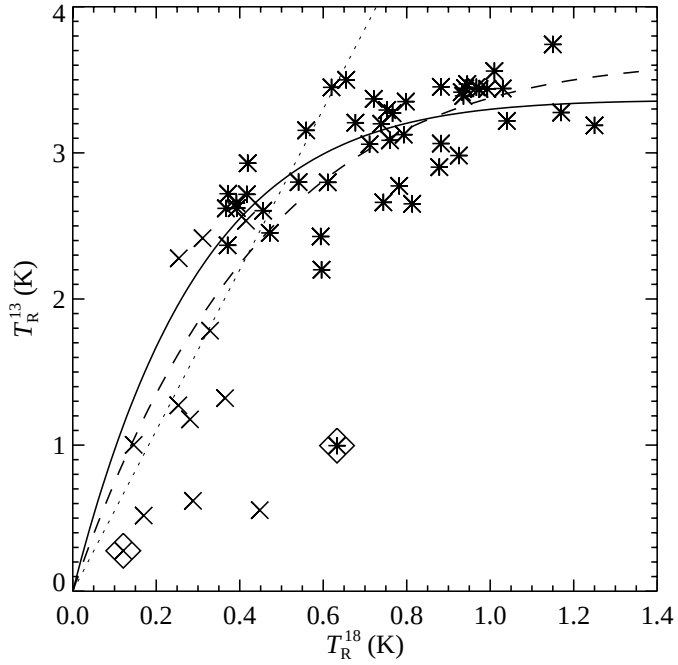

Fig. 2. T_R^{13} vs. T_R^{18} correlation plot. Intensities are taken from Gaussian fits to the spectra at the velocities of the $C^{18}O$ peaks. The solid line is the best fit of Eq. (3), using a non-weighted least-squares fit to all data points with SNR > 3 in both isotopes (asterisks). The curve implies a $^{13}CO/C^{18}O$ abundance ratio $X = 11.2$, and $T_{ex}(J = 1–0) = 8.0$ K. The dashed line is the fit to all data points (no SNR criterion, asterisks and crosses), yielding $X = 8.2$ and $T_{ex}(J = 1–0) = 8.4$ K. Box encompassed data points have velocity offsets >0.3 km s^{-1} between the lines of the two isotopes and are not used in these fits. For comparison, the dotted line gives the low-opacity relation for the terrestrial isotopic ratio $X = 5.5$.

2. the $^{13}CO/C^{18}O$ abundance ratio X is constant throughout the cloud, and
3. all the higher transitions of $C^{18}O$, i.e. $C^{18}O(J = 2–1, 3–2, \ldots)$ have the same excitation temperature $T_{ex}(J = 2–1)$, which may differ from $T_{ex}(J = 1–0)$.

This method, based on the modelling results of Warin et al. (1996), has been used earlier by Harjunpää (2002). The possibility that X can be constant within a cloud is supported by the results of Harjunpää & Mattila (1996) and Anderson et al. (1999) in CrA, where the $^{13}CO/C^{18}O$ and $H^{13}CO^+/HC^{18}O^+$ abundance ratios have an almost invariable value of 10.

4.1.2. Equations and results

The assumptions 1 and 2 lead to the following formula for the radiation temperatures at a certain velocity:

$$\frac{T_R^{13}}{T_\infty} = 1 - \left[1 - \frac{T_R^{18}}{T_\infty}\right]^X , \quad (3)$$

where T_R^{13} and T_R^{18} are the radiation temperatures of the $^{13}CO(J = 1–0)$ and $C^{18}O(J = 1–0)$ lines, respectively; T_∞ is defined by

$$T_\infty \equiv \frac{h\nu}{k}\left[f_\nu(T_{ex}) - f_\nu(T_{bg})\right] , \quad (4)$$

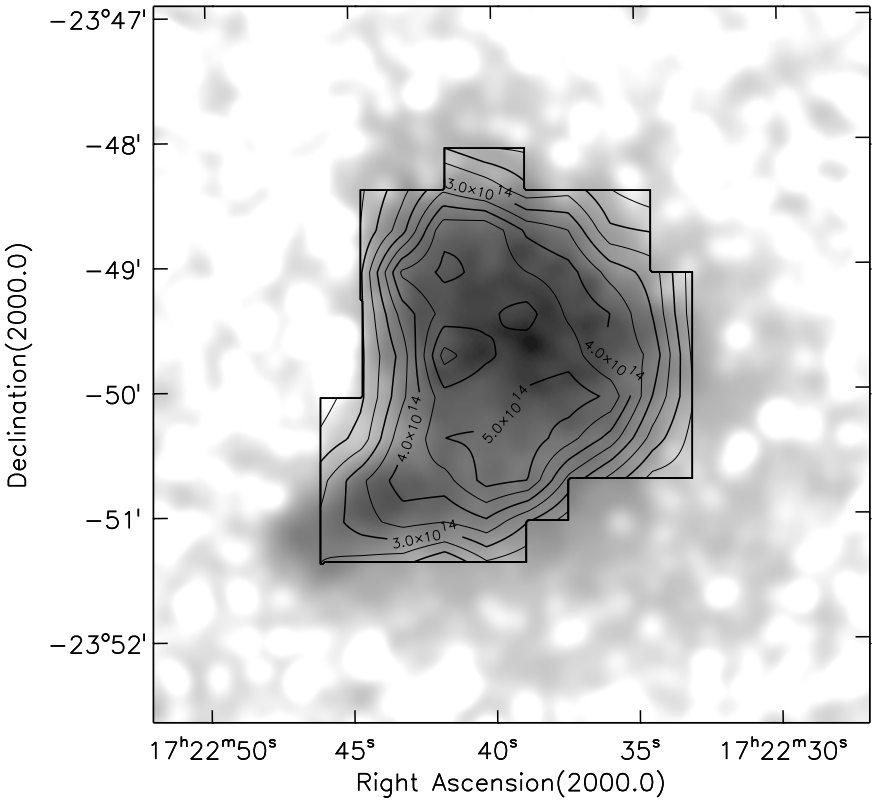

Fig. 3. $C^{18}O$ column densities (contours) overlaid on the POSS-II red plate (image). The optical image has been smoothed to 10″ resolution, and the transfer function is chosen to emphasise qualitatively the decrease in diffuse background brightness towards the centre of B68. The column densities are derived from our 2-transition observations of $C^{18}O$, assuming a constant (J = 1–0) excitation temperature of 8 K (see text and Fig. 2). The angular resolution is 50″. Only observed positions with an uncertainty $\Delta\left(N(C^{18}O)\right)/N(C^{18}O) < 30\%$ have been used for this map. Contours are drawn from 1.5 to 5.5×10^{14} cm^{-2} in steps of 0.5×10^{14} cm^{-2}, using alternating line thicknesses. The outer contours closely follow the optical outline of the globule. In the centre, the CO map is rather flat, while the diffuse light suggests an even further density increase. This behaviour is most likely to be due to CO depletion (see also Fig. 4).

and the function $f_\nu(T)$ is defined by

$$f_\nu(T) \equiv \frac{1}{e^{h\nu/kT} - 1}\ , \tag{5}$$

where ν is the transition frequency, h is the Planck constant, and k is the Boltzmann constant. In Fig. 2 we have plotted the observed ^{13}CO and $C^{18}O(J = 1–0)$ radiation temperatures at the velocities of the $C^{18}O$ peaks. The best fit of Eq. (3) to the data with $X = 11.2$ and $T_\infty = 3.4$ K is presented as a solid curve. The obtained value for T_∞ implies that $T_{ex}(J = 1–0) = 8.0$ K . To give an impression of the accuracy of the determined parameters, we also show a second fit (dashed line), which also uses data points of low signal-to-noise ratio (SNR). The value for X (now 8.2) is substantially lower, but $T_{ex}(J = 1–0)$ (now 8.4 K) differs by only 5%.

Using the derived value for $T_{ex}(J = 1–0)$, the excitation temperature $T_{ex}(J = 2–1)$ can be solved from the following equation for the observed $C^{18}O(J = 2–1)/(J = 1–0)$ integrated intensity ratio:

$$\frac{\int T_R(2–1)\mathrm{d}v}{\int T_R(1–0)\mathrm{d}v} = 2\,\frac{\nu_{21}}{\nu_{10}}\,e^{-h\nu_{21}/kT_{ex}(2–1)} \times \frac{1 - \frac{f_{\nu_{21}}(T_{bg})}{f_{\nu_{21}}(T_{ex}(2–1))}}{1 - \frac{f_{\nu_{10}}(T_{bg})}{f_{\nu_{10}}(T_{ex}(1–0))}}. \tag{6}$$

For this calculation, the two $C^{18}O$ data sets were convolved to a common 50″ Gaussian beam. The total $C^{18}O$ column density was calculated by using assumption 3. The derived distribution of the $C^{18}O$ column density is shown in Fig. 3. As can be seen in this figure, the column density distribution is relatively flat. The maximum is 5.5×10^{14} cm^{-2}, and the familiar figure of the cloud is outlined by the level 3.0×10^{14} cm^{-2}. In addition, the excitation temperature shows little variation in the central part of the cloud. The average $T_{ex}(J = 2–1)$ above the column density level 2.5×10^{14} cm^{-2} is 6.2 K and the sample standard deviation is 0.6 K.

4.1.3. Column density profile

We have plotted the radial distribution of the $C^{18}O$ column density in Fig. 4a. Also shown in this figure is the BES column density profile deduced from extinction measurements (see Sect. 2 and Alves et al. 2001). After convolving the BES column densities with a 2-dimensional 50″ (full width at half maximum) Gauss function, we can exclude a constant CO abundance in the gas phase. The difference between the measured and the smoothed profile strongly suggests CO depletion in the inner part of B68.

To quantify the observed depletion, we assume a depletion law of the form

$$f_d \equiv \frac{\widehat{Y}_{C^{18}O}}{Y_{C^{18}O}} = 1 + Z\left(\frac{n}{n_c}\right), \tag{7}$$

where the depletion factor f_d is an increasing function of gas density; we write $Y_{C^{18}O} \equiv n(C^{18}O, \mathrm{gas})/n(H_2)$ for the fractional $C^{18}O$ abundance and designate $\widehat{Y}_{C^{18}O} \equiv n(C^{18}O, \mathrm{gas + dust})/n(H_2)$ as the *no-depletion* fractional abundance. Equation (7) follows from the assumption that the fractional CO abundance is governed by accretion onto dust grains and desorption processes, which return

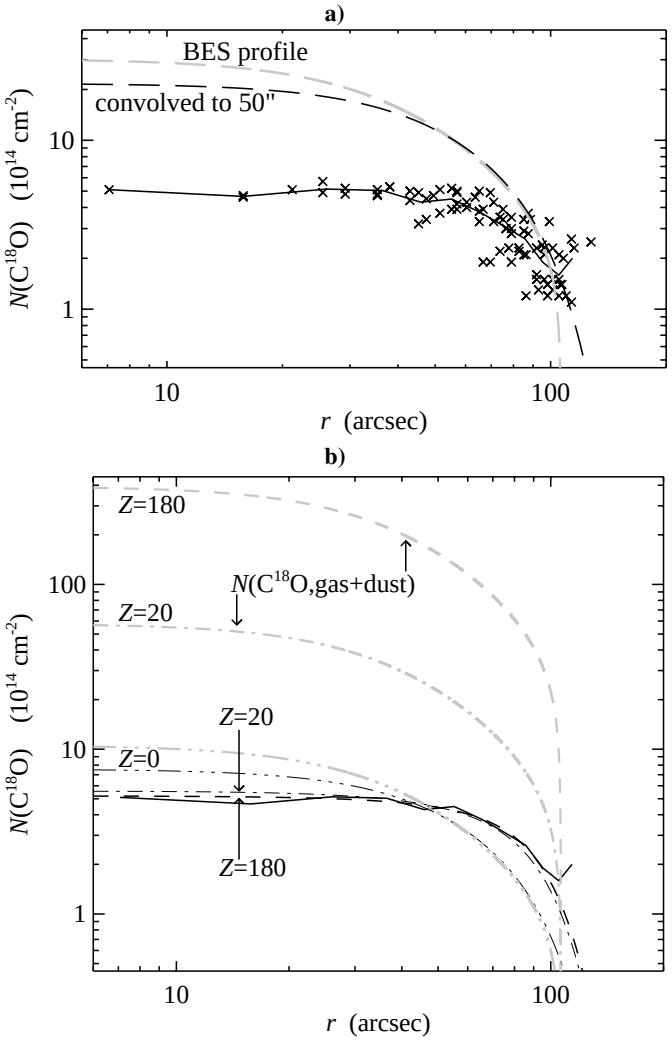

Fig. 4. a) $C^{18}O$ column density profile of B68. Crosses mark the same data points presented in the contour map of Fig. 3 (i.e. 50″ resolution, uncertainty <30%). The centre of the globule is at $\alpha(2000) = 17^h22^m40^s$, $\delta = -23°49'48''$. The solid line results from averaging over rings at intervals of 10″. For comparison, the long-dashed lines give the BES profile with $\xi_{max} = 7.0$ and angular radius 106″; black: convolved to our 50″ resolution, grey: unconvolved. The normalised theoretical profile is arbitrarily scaled in y-direction with a factor of 30.3. **b)** Assuming a depletion law according to Eq. (7), the depleted and smoothed profile is given as a black dashed line. The parameter Z in Eq. (7) and the scaling in y-direction were determined in a χ^2-fit to match the measured profile (solid line); individual measurements (crosses in **a**)) have been omitted for visibility. The scaling corresponds to a no-depletion curve as given by the grey dashed line (unsmoothed). While the dashed lines show the best-fitting depletion model ($Z = 180$ yields the lowest χ^2), the other lines show profiles for other values of Z; dash-dot: $Z = 20$; dash-dot-dot-dot: $Z = 0$. In all cases, the grey lines show the unconvolved total (gas+dust) $C^{18}O$ column densities.

the molecules into the gas phase. The accretion rate in an isothermal cloud is $A\, n(C^{18}O, \mathrm{gas})\, n(H_2)$, while the desorption rate can be written in the form $B\, n(C^{18}O, \mathrm{dust})$. The adsorption and desorption coefficients A and B depend primarily on grain properties, temperature and the flux of heating particles, as discussed in Sect. 6.1. In a steady state condition the relation $A\, n_{H_2}^2\, Y_{C^{18}O} = B\, n_{H_2}\, (\widehat{Y}_{C^{18}O} - Y_{C^{18}O})$ holds, and hence

$$f_d = 1 + \left(\frac{A}{B}\right) n(H_2)\,. \tag{8}$$

Without knowing what n_c actually is, we can determine Z from Fig. 4, calculating later $A/B = Z/(n_c \cdot n(H_2)/n)$; we assume $n(H_2)/n$ to be 5/6 (Sect. 2).

Starting from the BES density profile, we first calculated a depleted column density distribution for various values of Z, then smoothed the results to our 50″ resolution. Finally, we used the χ^2-method to scale the theoretical depleted profile to the measured profile, which corresponds to determining $N_c(C^{18}O, \mathrm{gas + dust})$. Figure 4b shows the profile with the lowest χ^2, which has $Z = 180$ and $N_c(C^{18}O, \mathrm{gas + dust}) = 3.9 \times 10^{16}$ cm^{-2}. This profile reproduces the observed profile from $r = 20''$ to $r = 100''$ almost perfectly. For small values of Z the fits quickly become worse, with χ^2 increasing by 15% for $Z = 50$ and by 100% for $Z = 20$. Larger values of Z cannot be excluded from the depletion analysis alone, because χ^2 increases by only a few percent for $Z = 180 \rightarrow \infty$. This is so because for very large Z the scaling (which determines the gas+dust abundance) can compensate any futher increase in Z. Only by requiring that $\widehat{Y}_{C^{18}O}$ does not rise into physically unrealistic regimes we can give an upper limit for Z, which will be discussed in Sect. 6.

4.2. Monte Carlo simulations

We constructed a series of isothermal model clouds with kinetic temperatures between 6 and 16 K and distances between 40 and 300 pc, all with a BES-like density distribution ($\xi_{max} = 7.0$ and $\theta_R = 106''$). The radiative transfer problem was solved with Monte Carlo methods (Juvela 1997). The radiation field was simulated with a large number of model photons resulting from background radiation and emission from within the cloud, where a microturbulent velocity field was assumed. The simulations were used to determine the radiation field in each of the 40 spherical shells into which the model was divided and to derive new estimates for the level populations of the molecules. The whole procedure was iterated until the relative change in the level populations were $\sim 10^{-4}$ between successive iterations.

The observed $C^{18}O$ spectra were averaged over rings at intervals of 20″ at distances 0″ to 100″ from the selected centre position RA $17^h19^m37\overset{s}{.}1$, Dec $-23°46'59''$ (1950.0). The effective resolution of the averaged $C^{18}O(J = 1–0)$ and $(J = 2–1)$ spectra are 60″ and 30″ respectively. Corresponding spectra were calculated from the models and averaged with a Gaussian beam to the resolution of the observations. The correspondence between the observed spectra and the model was measured with a χ^2 value summed channel by channel over all spectra. Averaged spectra at different distances from the centre position were all given equal weight in the fit.

For each pair of T and D, two parameters were optimised: the fractional $C^{18}O$ abundance $Y_{C^{18}O}$ and the turbulent line width. The best fit was obtained for $T_{kin} = 6$ K and $D = 80$ pc with $Y_{C^{18}O} = 6.9 \times 10^{-8}$. However, this solution still produces

far too little intensity at large offsets, the observed intensity at 100″ being more than twice the model prediction.

We further studied a series of models assuming a non-constant $C^{18}O$ fractional abundance, $Y_{C^{18}O} \equiv Y_{C^{18}O}(n)$, in order to account for CO depletion in the cloud centre. The density dependency was assumed to be $Y_{C^{18}O} = \widehat{Y}_{C^{18}O}/(1 + Z\,n/n_c)$, as suggested in the homogenuous model analysis (Sect. 4.1.3). For the depletion parameter Z we tried a large range of values between 4 and 10^4.

As in Sect. 4.1.3, we find Z not to be well constrained, lying somewhere between 20 and 300. In contrast to our earlier analysis, we now do find an upper limit for Z, just as we can give a lower limit. The reason for this is that in the homogenuous approach, high densities n, which go along with a high Z, do not influence the excitation conditions (T_{ex} being determined earlier), while now the total density n and not only $n(C^{18}O)$ is taken into account.

For both $Z = 50$ and $Z = 200$, the best fitting values for the distance and the temperature are 70 pc and 7 K respectively. Some other specific combinations of Z, D and T within the ranges $Z = 20$–200, $D = 70$–120 pc and $T = 6$–8 K result in almost equally good fits. The Monte Carlo simulations do not favour a particular model, as the χ^2 values are not significantly different. They do, however, favour the models including depletion as compared to the $Z = 0$ ones. For Z in the given range the χ^2 values are a factor of 1.6 lower than in the no-depletion models, and the spectra are well fitted from the centre out to the edge of the cloud. Figure 5 shows the correspondence between the model and the observed spectra.

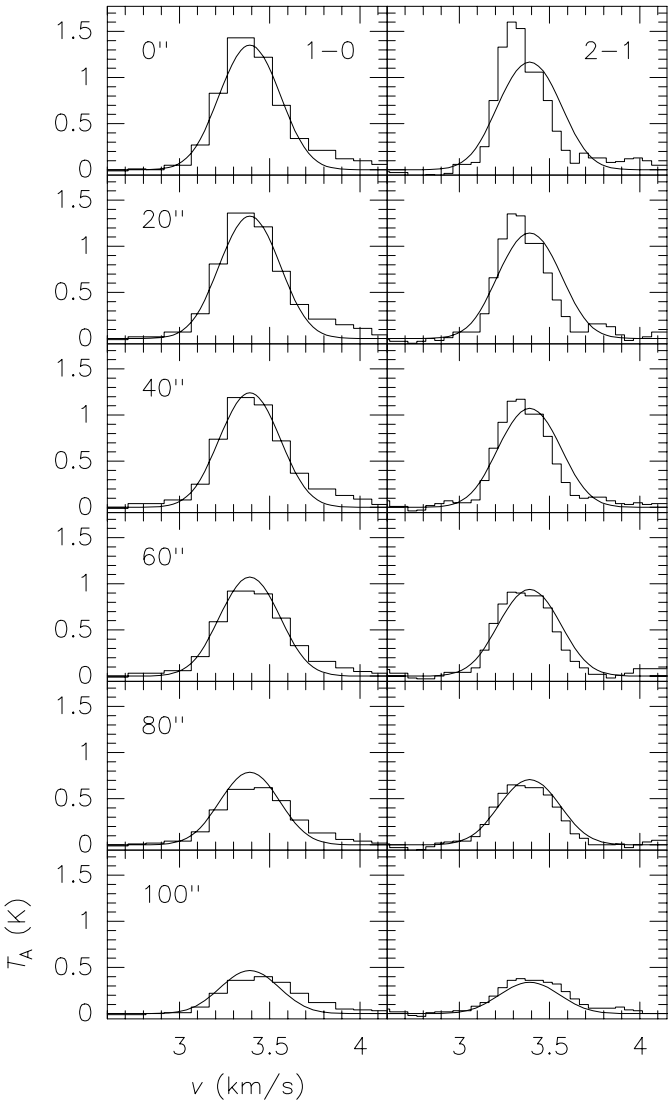

Fig. 5. Comparison of observed and modelled spectra. The observed spectra (histograms) are averages over rings at distances between 0″ and 100″ from the centre. The modelled spectra (smooth lines) are generated using Monte Carlo simulations as described in the text. The $C^{18}O(J = 1$–$0)$ transition is shown in the left column, $C^{18}O(J = 2$–$1)$ in the right column. Each row stands for one angular distance from the centre. The model behind the simulation presented in this figure is an isothermal cloud with BES-like density structure at 70 pc distance with a kinetic temperature of 7 K and CO depletion according to Eq. (7) with $Z = 200$.

5. Deriving H_2 column densities from $E(H - K)$

In order to estimate the column density profile of B68, Alves et al. (2001) derived the colour excesses $E(H - K)$ of more than a thousand background stars behind the cloud (the underlying assumption is that $E(H - K) \propto N_{gas}$). Referring to the standard, i.e. $R_V = 3.1$, interstellar reddening law of Mathis (1990), they used the relationship $A_V = 14.67\,E(H - K)$ to plot the visual extinction profile. By convention, A_V is used to present extinction or reddening data. A_V is however not the best parameter to be converted to hydrogen column density, because the conversion factor depends on grain properties, which can be different in different environments (Kim & Martin 1996). We therefore use $E(H - K)$ for converting the extinction data to gas column density. The best fitting BES extinction profile reaches $A_V = 30.3$ mag (Sect. 2), hence follows $E(H - K) = 2.07$ mag in the centre of the globule.

From UV observations in the direction of diffuse clouds Bohlin et al. (1978) determined the relation between reddening in the optical and hydrogen column density:

$$\frac{N(\mathrm{H\,I}) + 2N(\mathrm{H_2})}{E(B - V)} = 5.8 \times 10^{21}\ \mathrm{cm^{-2}\ mag^{-1}}. \quad (9)$$

This relationship (Eq. (9)), which is frequently used in "scaling" the dust column densities to $N(H_2)$, may be seriously in error in the case of dense clouds. Practically no dense-cloud lines of sight were included in the sample of Bohlin et al. (1978). Diplas & Savage (1994) re-examined the ratio $N(\mathrm{H\,I})/E(B - V)$ for a larger sample of sight lines. They found that the ratio increases to a value of 7.8×10^{21} cm^{-2} mag^{-1} ± 12%, for sight lines involving target stars located in dusty regions where $n(\mathrm{H\,I}) > 1.5$ cm^{-3}. This increase is also expected for theoretical reasons, since a depletion of small particles in dense clouds leads to a reduced reddening efficiency (see e.g. Kim & Martin 1996). A counter-example are two obscured lines of sight, studied recently by the Far Ultraviolet Spectroscopic Explorer (FUSE), i.e. HD 73882 with $A_V = 2.44$ mag (Snow et al. 2000) and HD 110432 behind the Coalsack dark nebula with $A_V = 1.32$ mag (Rachford et al. 2001). For these two lines of sight, the numerical factor in

Eq. (9) is 5.1 (HD 73882) and 4.2 (HD 110432) instead of 5.8. The conclusion is that there is no evidence for a substantial increase in the H_2-to-extinction ratio towards those "translucent lines of sight" in denser dust clouds which can still be studied by means of ultraviolet observations.

Cardelli et al. (1989) derived a family of extinction laws for both diffuse and dense regions, parameterised by the total-to-selective extinction ratio $R_V = A_V/E(B-V)$. Their extinction curve for the canonical value $R_V = 3.1$, which is an average for lines of sight penetrating the *diffuse* interstellar medium, results in the colour excess ratio

$$\frac{E(H-K)}{E(B-V)} = 0.236. \quad (10)$$

In the case of dense dark clouds, where all hydrogen is in molecular form, Eqs. (9) and (10) lead to

$$\frac{N(H_2)}{E(H-K)} = 1.23 \times 10^{22}\ \mathrm{cm^{-2}\ mag^{-1}}\ . \quad (11)$$

We apply this to B68 and obtain

$$N_c(H_2) = 2.5 \times 10^{22}\ \mathrm{cm^{-2}} \quad (12)$$

in the centre of the globule, keeping in mind that Eq. (11) is ultimately derived from the diffuse dust sample of Bohlin et al. (1978).

Even though there is reason to assume the extinction law at near-infrared (NIR) wavelengths to be independent of environment (Mathis 1990), the normalisation of the extinction curve (with respect to hydrogen column density) may still show a dependency. Observational evidence either favouring or opposing the latter dependency would help to assess the applicability of Eq. (11) to B68, but is still scarce. The $(N(\mathrm{H\,I}) + 2N(H_2))/E(H-K)$ ratio determined towards ρ Oph A(HD 147933), which is seen through an extinction layer of $E(B-V) = 0.47$ mag on the outskirts of the dense ρ Oph cloud core, is close to the value indicated in Eq. (11) (de Boer et al. 1986; Clayton & Mathis 1988).

Using NIR spectroscopy, H_2 column densities can be probed in much denser clouds. Lacy et al. (1994) have detected the $H_2(v = 1\text{–}0)\,S(0)$ line (4498 $\mathrm{cm^{-1}}$) in absorption towards NGC2024 IRS2, and they derive $N(H_2) = 3.5 \pm 1.4 \times 10^{22}\ \mathrm{cm^{-2}}$. By modelling the observed spectral energy distribution of IRS2 at 1.65, 2.2, and 4.64 μm, Jiang et al. (1984) have derived a colour excess of $E(H-K) = 1.5 \pm 0.3$ mag in this direction (using extinction curve No. 15 of van de Hulst 1957). Furthermore, Maihara et al. (1990) have observed the Brα/Brγ line ratio towards the compact H II region surrounding IRS2. The resulting colour excess is $E(\mathrm{Br}\gamma - \mathrm{Br}\alpha) = 1.31 \pm 0.13$ mag, which corresponds to $E(H-K) = 1.35 \pm 0.14$ mag (Cardelli et al. 1989). Adopting the mean of these two colour excesses, we end up with the ratio

$$\frac{N(H_2)}{E(H-K)} = 2.5 \pm 1.1 \times 10^{22}\ \mathrm{cm^{-2}\ mag^{-1}}. \quad (13)$$

This ratio is ∼2 times larger than the diffuse dust value (Eq. (11)). However, the uncertainties are large, and the lower limit of Eq. (13) is close to the value in Eq. (11). Moreover, because the value in Eq. (13) is still based on a single source we cannot adopt it as a proven observational result. It does suggest, however, that the H_2-to-extinction ratio may increase in dense cloud cores (even for NIR extinction), and the use of Eq. (11) for B68 may result in an underestimate of $N(H_2)$.

6. Discussion

6.1. $C^{18}O$ abundance distribution

In pure gas-phase chemistry models the CO abundance is very stable. At gas densities over 10^3 $\mathrm{cm^{-3}}$ it is practically constant at all times. Therefore, any variation in the fractional CO abundance observed in B68 is probably due to accretion and desorption processes on dust grains. The adopted CO depletion law, as described in Sect. 4.1.3, is consistent with a steady state, i.e. with the situation where accretion and desorption are in equilibrium. In the time-dependend depletion model of Caselli et al. (2001) this situation corresponds to very late stages of chemical evolution. One plausible theory of the origin of globules is that they are remnants of dense cores of dark clouds or cometary globules (Reipurth 1983). This scenario supports the possibility that B68, being an aged object, could indeed have reached chemical equilibrium.

The assumption that A/B is constant includes the following assumptions: 1) The gas kinetic temperature is roughly constant, 2) the dust temperature remains everywhere below the critical temperature of CO desorption, which lies in the range 20–30 K (Léger et al. 1985; Takahashi & Williams 2000), and 3) the same desorption mechanisms are operating throughout the cloud. The constancy of the gas temperature is already built in the adopted physical model (first assumption). The average dust temperature of B68 is ≈13 K, which we have derived using ISOPHOT Serendipity Survey data (for calibration see Hotzel et al. 2001). Langer & Willacy (2001) claim the detection of a dust core of 8–9 K. Both observational results support the validity of the second assumption.

As discussed in detail by Watson & Salpeter (1972), Léger et al. (1985), Willacy & Millar (1998) and Takahashi & Williams (2000), the desorption mechanisms operating in dense dark clouds with no star formation are connected with cosmic rays, X-rays or H_2 formation on grains. The main process in all three cases is impulsive whole grain or spot heating, resulting in classical evaporation of adsorbed molecules. Cosmic rays can also contribute to desorption via chemical explosions, and via photo-desorption by UV photons resulting from excitation of H_2 molecules, but both processes are believed to be effective in the low extinction regions only (Léger et al. 1985). These processes are neglected hereafter, as is heating due to H_2 formation on grains because of its relative inefficiency compared with cosmic ray heating (Takahashi & Williams 2000). According to Léger et al. (1985) X-rays can heat small grains with radii in the range 200–400 Å more efficiently than cosmic rays, while the heating of larger grains is assumed to be dominated by cosmic rays.

The accretion and desorption constants are actually integrals over the grain cross section distribution and the velocity or energy distributions of the colliding particles. The accretion

constant can be written as $A = 2\epsilon\langle v\rangle S$, where ϵ is the total dust grain surface area per H nucleon, $\langle v\rangle$ is the average speed of the molecules in question (at 8 K: $\langle v(C^{18}O)\rangle = 7.5 \times 10^3$ cm s^{-1}) and S is the sticking probability, which is generally assumed to be unity in cold clouds (e.g. Sandford & Allamandola 1990). The factor of 2 comes from the assumption that all hydrogen is in molecular form. The value of ϵ depends on the assumed grain size distribution, and especially on the lower cut off of the grain radius, a_-. For example, the distribution adopted by Léger (1983), with $a_- = 50$ Å, gives $\epsilon = 1.4 \times 10^{-21}$ cm^2. On the other hand, if one assumes that CO on grains with radii below 400 Å is efficiently desorbed by X-rays or by other processes (i.e. effectively no absorption on small grains), the effective ϵ becomes 3.5×10^{-22} cm^2. The accretion constants A corresponding to these ϵ-values are 2.1×10^{-17} cm^{-3} s^{-1} and 5.3×10^{-18} cm^{-3} s^{-1}.

Based on the work of Léger et al. (1985) and Hasegawa & Herbst (1993), Caselli et al. (2001) assumed that the desorption in L1544 is dominated by thermal evaporation due to heating by relatively heavy cosmic rays. The cosmic ray desorption rate for CO derived by Hasegawa & Herbst (1993), $k_{\rm CRD}(\rm CO) = 9.8 \times 10^{-15}$ s^{-1}, is based on the Fe nuclei flux derived by Léger et al. (1985), which is consistent with a total H_2 ionization rate of 10^{-17} s^{-1}. Other assumptions used for the indicated value of $k_{\rm CRD}$ are that 1) the average grain radius is about 1000 Å (needed for the calculation of the fraction of the time spent by grains in the vicinity of 70 K), 2) the adsorption energy of CO is 1210 K and 3) that the characteristic adsorbate vibrational frequency of CO is 10^{12} s^{-1}. The uncertainty of the cosmic ray desorption rate is a good order of magnitude (Caselli et al. 2001).

Assuming that the mentioned process dominates the replenishment of gas-phase CO, we set $B = k_{\rm CRD}(\rm CO)$ and use the accretion constant for $a_- = 400$ Å. Then we get $A/B = 5.4 \times 10^{-4}$ cm^{-3}, and the corresponding value of the parameter $Z = \frac{5}{6} n_{\rm c}\, A/B$ is about 100. In view of the large uncertainty of the desorption constant, all Z values from ~10 to 10^3 fit the model of Hasegawa & Herbst (1993).

The modelling of the parameter Z to the observed column density profile in Sect. 4.1.3 gave a best fit for $Z = 180$ and the fit became noticeably worse for $Z \sim 50$. We must consider values down to $Z = 20$ however, as the Monte Carlo analysis in Sect. 4.2 still produced good results for this number. The latter modelling also set the upper bound to $Z \sim 300$, but an even tighter limit is set from the cosmic abundances of H, C and ^{18}O: With the solar abundance $[\rm C]/[H] = 4.7 \times 10^{-4}$ (Lambert 1978) and the terrestrial isotopic ratio $[^{16}O]/[^{18}O] = 489$ (Duley & Williams 1984, p.175), we get $\widehat{Y}^{\rm max}_{C^{18}O} = 1.9 \times 10^{-6}$. For B68, with $N_{\rm c}(H_2) = 2.5 \times 10^{22}$ cm^{-2} (Eq. (12)), this means $N_{\rm c}^{\rm max}(C^{18}O, \text{gas + dust}) = 4.8 \times 10^{16}$ cm^{-2}. This number is reached for $Z \approx 200$ (see Fig. 4b). For our lower limit $Z = 20$ we find $N_{\rm c}(C^{18}O, \text{gas + dust}) = 0.6 \times 10^{16}$ cm^{-2}, corresponding to 13% of carbon nuclei being bound in CO molecules. More recent determinations of solar and stellar carbon abundances suggest that the average galactic value is a factor of 2 lower than the value of Lambert (1978) used above (see discussion in Snow & Witt 1995). Therefore, even though a relatively high [C]/[H] ratio may be present in B68 (as in the sun), it is save to exclude Z values exceeding 200.

The reasonable Z range derived from our observations is thus $20 < Z < 200$, corresponding to only 5% to 0.5% of all CO molecules in the centre of B68 being in the gas phase. The large overlap with the above prediction deduced from the model of Hasegawa & Herbst (1993) suggests that the degree of CO depletion can indeed be understood in terms of accretion and cosmic ray induced desorption.

The derived range for $\widehat{Y}_{C^{18}O}$ is considerably higher than the commonly quoted fractional abundance value $Y_{C^{18}O} = 1.7 \times 10^{-7}$ of Frerking et al. (1982), which is based on a CO vs. A_V comparison in the ρ Ophiuchus and Taurus molecular cloud complexes. This is to be expected because they ultimately measured the gas phase CO. To compare our results with their value, we have calculated the gas-phase fractional abundance at the outer boundary: $n_{\rm R}(C^{18}O, \text{gas})/n_{\rm R}(H_2) = 1.6 \times 10^{-3}/1.5 \times 10^4 = 1.1 \times 10^{-7}$. This value lies between the values of Frerking et al. (1982) for Taurus "envelopes" (0.7×10^{-7}) and "dense cores" (1.7×10^{-7}). Considering that $Y_{C^{18}O}$ drops towards the centre of B68, we would have observed a lower fractional abundance if we had directly used *column* densities, as has been done in most other studies. Therefore, our value is comparable to the value for the Taurus envelopes. Harjunpää & Mattila (1996) investigated the molecular clouds Chamaeleon I, R Coronae Australis and the Coalsack and determined the $N(C^{18}O)$ vs. $E(J-K)$ relations, corresponding to fractional abundances $Y_{C^{18}O}$ between 0.7×10^{-7} (Coalsack) and 2×10^{-7} (Chamaeleon I). $Y_{C^{18}O}$ is clearly lower in B68 than it is in the active star forming regions R Coronae Australis, Chamaeleon I and ρ Ophiuchus. This points towards a possible relation between the depletion degree and the star formation activity.

6.2. Temperature and distance

As discussed in Sect. 2, the concept of Bonnor-Ebert spheres imposes Eq. (1) on the relation between certain observable parameters. Assuming that the state of isothermal hydrostatic equilibrium does apply to B68, we can derive its distance and mass from Eq. (2) if the kinetic temperature and the central column density are known.

There are several reasons to doubt the high kinetic temperature of 16 K derived by Bourke et al. (1995). The first comes from their own results. By using this kinetic temperature and the excitation temperature of the $(J, K) = (1, 1)$ inversion transition of NH_3, they derive a hydrogen number density of $n(H_2) = 9.1 \times 10^3$ cm^{-3}. This is a good order of magnitude lower than the value from the BES model. According to Eq. (2) of Ho & Townes (1983), an overestimate of the kinetic temperature leads to an underestimate of the H_2 number density, which suggests that Bourke et al. (1995) used a too high value for $T_{\rm kin}$. Secondly, our observations and Monte Carlo modelling results are in agreement with the assumption of a nearly homogenous excitation temperature of $T_{\rm ex}(J = 1\text{–}0) = 8$ K for ^{13}CO and $C^{18}O$, which in turn is roughly equal to $T_{\rm kin}$. These results agree with the earlier observations of Avery et al. (1987). Moreover,

temperatures derived from ammonia in other globules without internal heating sources lie at around 10 K (Lemme et al. 1996). Finally, the modelling results of Zucconi et al. (2001) for a BES with similar characteristics to B68 suggest that the dust temperature decreases well below 10 K in the dense inner parts, which is consistent with a low gas temperature in such an object.

After taking $T = 8$ K as the most likely kinetic temperature, the distance can be checked by using the formula for the central column density $N_c (= 1.2N(H_2))$ in Eq. (2) and the canonical $N(H_2)/E(H-K)$ ratio given in Eq. (11). As the NIR reddening at the cloud center is $E(H-K) = 2.07$ mag, we find that the distance to the cloud is about 70 pc. The adoption of the non-standard ratio given in Eq. (13) would bring the cloud still nearer, which would however be unlikely on the basis of the Monte Carlo results (see Sect. 4.2). Therefore, it seems reasonable to assume that the cloud is located on the near side of the Ophiuchus complex, i.e. at a distance of 80 pc (de Geus et al. 1989).

Summarizing, $T = 8$ K and $D = 80$ pc are the most likely values that are consistent with B68 being a Bonnor-Ebert sphere and our own observations. This is the first distance estimate ever for this globule, which is not based on the ad hoc assumption that B68 is at the same distance as the centre of the Ophiuchus giant molecular cloud complex. The small distance and temperature values imply a significantly lower mass than previously estimated: The parameters of B68 as calculated by Eq. (2) are $n_c = 2.61 \times 10^5$ cm^{-3}, $N_c = 2.59 \times 10^{22}$ cm^{-2}, $M = 0.67\ M_\odot$ and $P_R = 1.69 \times 10^{-12}$ Pa. The derived value for the external pressure, which is needed to contain the BES, is not too far away from the pressure of the Loop 1 superbubble ($0.9–1.2 \times 10^{-12}$ Pa, Breitschwerdt et al. 2000).

7. Summary

We have mapped B68 in $^{13}CO(J = 1–0)$, $C^{18}O(J = 1–0)$ and $C^{18}O(J = 2–1)$. Combining our observations with the extinction profile of B68 (Alves et al. 2001), which closely follows the one predicted for a Bonnor-Ebert sphere, we have come to the following results:

1. The kinetic temperature of the gas is ≈8 K.
2. The density dependence of the $C^{18}O$ abundance distribution proves substantial molecular depletion in B68. The CO depletion factor f_d is well fitted with the law $f_d = 1 + n(H_2)\,A/B$. The agreement between the estimates for the ratio of the accretion constant and the depletion constant, A/B, based on previous model predictions and derived from our measurements, suggests that the degree of CO depletion can be understood in terms of accretion onto dust grains and cosmic ray induced desorption. In the centre of B68, between 0.5% and 5% of all CO molecules remain in the gas phase.

Based on the assumption that B68 is indeed a BES, i.e. being isothermal and in hydrostatic equilibrium, we conclude futhermore:

3. The most likely distance to B68 is ≈80 pc.
4. The mass of the globule is ≈0.7 $M_\odot$, which is considerably less than estimated previously on the basis of other distance and temperature values.
5. The near-infrared reddening efficiency of dust grains per unit H_2 column density is close to the canonical value derived in diffuse clouds. A clearly higher reddening efficiency would disagree with our observations.

Acknowledgements. We thank Dr. João F. Alves for providing us with the data of the measured extinction profile of B68. The Second Palomar Observatory Sky Survey (POSS-II) was made by the California Institute of Technology with funds from the National Science Foundation, the National Geographic Society, the Sloan Foundation, the Samuel Oschin Foundation, and the Eastman Kodak Corporation. This project was supported by Deutsches Zentrum für Luft- und Raumfahrt e. V. (DLR) with funds of Bundesministerium für Bildung und Forschung, grant No. 50 QI 9801 3, and by the Academy of Finland, grant Nos. 173727 and 174854.

References

Alves, J. F., Lada, C. J., & Lada, E. A. 2001, Nature, 409, 159
Anderson, I. M., Caselli, P., Haikala, L. K., & Harju, J. 1999, A&A, 347, 983
Avery, L. W., White, G. J., Williams, I. P., & Cronin, N. 1987, ApJ, 312, 848
Bally, J., & Langer, W. D. 1982, ApJ, 255, 143
Barnard, E. E. 1919, ApJ, 49, 1
Bohlin, R. C., Savage, B. D., & Drake, J. F. 1978, ApJ, 224, 132
Bok, B. J., & McCarthy, C. C. 1974, AJ, 79, 42
Bonnor, W. B. 1956, MNRAS, 116, 351
Bourke, T. L., Hyland, A. R., Robinson, G., James, S. D., & Wright, C. M. 1995, MNRAS, 276, 1067
Breitschwerdt, D., Freyberg, M. J., & Egger, R. 2000, A&A, 361, 303
Cardelli, J. A., Clayton, G. C., & Mathis, J. S. 1989, ApJ, 345, 245
Caselli, P., Walmsley, C. M., Tafalla, M., Dore, L., & Myers, P. C. 1999, ApJ, 523, L165
Caselli, P., Walmsley, C. M., Terzieva, R., & Herbst, E. 1998, ApJ, 499, 234
Caselli, P., Walmsley, C. M., Zucconi, A., et al. 2001 [astro-ph/0109023]
Chandrasekhar, S. 1939, An introduction to the study of stellar structure (The University of Chicago press, Chicago, Illinois)
Chini, R. 1981, A&A, 99, 346
Clayton, G. C., & Mathis, J. S. 1988, ApJ, 327, 911
Clemens, D. P., & Barvainis, R. 1988, ApJS, 68, 257
de Boer, K. S., Lenhart, H., van der Hucht, K. A., et al. 1986, A&A, 157, 119
de Geus, E. J., de Zeeuw, P. T., & Lub, J. 1989, A&A, 216, 44
Diplas, A., & Savage, B. D. 1994, ApJ, 427, 274
Duley, W. W., & Williams, D. A. 1984, Interstellar Chemistry (London: Academic Press)
Ebert, R. 1955, Z. Astrophys., 37, 217
Frerking, M. A., Langer, W. D., & Wilson, R. W. 1982, ApJ, 262, 590
Harjunpää, P. 2002, A&A, in preparation
Harjunpää, P., & Mattila, K. 1996, A&A, 305, 920
Hasegawa, T. I., & Herbst, E. 1993, MNRAS, 261, 83
Ho, P. T. P., & Townes, C. H. 1983, ARA&A, 21, 239
Hotzel, S., Harju, J., Lemke, D., Mattila, K., & Walmsley, C. M. 2001, A&A, 372, 302
Jiang, D. R., Perrier, C., & Léna, P. 1984, A&A, 135, 249
Juvela, M. 1997, A&A, 322, 943
Kim, S., & Martin, P. G. 1996, ApJ, 462, 296

Lacy, J. H., Knacke, R., Geballe, T. R., & Tokunaga, A. T. 1994, ApJ, 428, L69
Lambert, D. L. 1978, MNRAS, 182, 249
Langer, W. D., & Willacy, K. 2001, ApJ, 557, 714
Léger, A. 1983, A&A, 123, 271
Léger, A., Jura, M., & Omont, A. 1985, A&A, 144, 147
Lemme, C., Wilson, T. L., Tieftrunk, A. R., & Henkel, C. 1996, A&A, 312, 585
Lynds, B. T. 1962, ApJS, 7, 1
Maihara, T., Mizutani, K., & Suto, H. 1990, ApJ, 354, 549
Mathis, J. S. 1990, ARA&A, 28, 37
Rachford, B. L., Snow, T. P., Tumlinson, J., et al. 2001, ApJ, 555, 839
Reipurth, B. 1983, A&A, 117, 183
Sandford, S. A., & Allamandola, L. J. 1990, Icarus, 87, 188
Smith, D., & Adams, N. G. 1984, ApJ, 284, L13
Snow, T. P., Rachford, B. L., Tumlinson, J., et al. 2000, ApJ, 538, L65
Snow, T. P., & Witt, A. N. 1995, Science, 270, 1455
Straizys, V. 1984, Vilnius Astronomijos Observatorijos Biuletenis, 67, 15
Takahashi, J., & Williams, D. A. 2000, MNRAS, 314, 273
Tielens, A. G. G. M., Tokunaga, A. T., Geballe, T. R., & Baas, F. 1991, ApJ, 381, 181
van de Hulst, H. C. 1957, Light Scattering by Small Particles (New York: John Wiley & Sons)
Warin, S., Benayoun, J. J., & Viala, Y. P. 1996, A&A, 308, 535
Watson, W. D., & Salpeter, E. E. 1972, ApJ, 174, 321
Willacy, K., & Millar, T. J. 1998, MNRAS, 298, 562
Zhou, S., Wu, Y., Evans, N. J., Fuller, G. A., & Myers, P. C. 1989, ApJ, 346, 168
Zucconi, A., Walmsley, C. M., & Galli, D. 2001 [astro-ph/0107055]